

Vertebrae segmentation, identification and localization using a graph optimization and a synergistic cycle

Di Meng*, Eslam Mohammed, Edmond Boyer, Sergi Pujades

Inria, Univ. Grenoble Alpes, CNRS, Grenoble INP, LJK, France

Abstract

This paper considers the segmentation, identification and localization of vertebrae in CT images. Although these three tasks are related, they face specific problems that add up when they are addressed together. For example neighboring vertebrae with similar shapes perturb the identification and vertebrae with complex or even pathological morphologies impact the segmentation. Consequently, the three tasks tend to be approached independently, e.g. labelling (localization and identification) or segmenting only, or, when treated globally, a sequential strategy is used. Sequential methods however are prone to accumulate errors as they are not able to recover from mistakes of the previous module. In this work, we propose to combine all three tasks and leverage their interdependence : locations ease the segmentation, the segmentations in turn improve the locations and they all contribute and benefit from the identification task. To this purpose we propose a virtuous cycle to enforce coherence between the three tasks. Within such a cycle, the tasks interoperate and are iterated until a global consistency criterion is satisfied. Our experiments validate this strategy with anatomically coherent results that outperform the state of the art on the VerSe20 challenge benchmark. Our code and model are openly available for research purposes¹.

Keywords: Spine, Vertebrae, Segmentation, Labelling

1. Introduction

Segmenting, identifying and localizing vertebrae in CT images play an essential role in many clinical applications, such as the spinal deformities assessment (Forsberg et al., 2013) or computer-assisted surgical interventions (Merloz et al., 1998; Knez et al., 2016). All these tasks deal with vertebrae shape information and are faced with several task-specific critical challenges : i. Neighboring vertebrae can have similar shapes which makes it difficult to robustly identify and localize them ; ii. The number of vertebrae can change among patients. While most humans have 12 thoracic vertebrae, some present 11 or 13. Similarly, some humans have 6 lumbar vertebrae instead of 5. These rare cases make the identification and localization particularly challenging ; iii. Pathological spines, e.g. suffering from bone calcification or broken vertebrae, can present abnormal shapes that affect the segmentation tasks ; iv. Given arbitrary field of view CT images, counting vertebrae is suboptimal (Lessmann et al., 2019) when no distinctive vertebra is available in the observation which, again, impacts the identification. Our method is designed to deal with these challenges by combining a local approach, aiming at identifying individual vertebrae,

with a global reasoning enforcing the anatomic consistency among the individual predictions. As mentioned earlier, the segmentation of individual vertebra is difficult as a result of the complex morphology of the vertebrae as well as of the tissue non-homogeneity arising from bone pathological cases. Our method provides a segmentation-location refinement step that simultaneously optimizes the location of each individual vertebra and its final segmentation mask.

In most existing works, vertebrae labeling and segmentation are treated either independently or with a chain of modules that address the tasks in a sequential manner, hence benefiting from some partial consistency between tasks while limiting error propagation within each module. In this paper we investigate this consistency process further and propose a synergistic cycle in which all three tasks collaborate and complement each other : initial vertebrae locations are used to compute individual segmentations. The associated segmentation masks ease the vertebrae identification which, in turn, helps finding missing locations. These steps are iterated, recovering from potential mistakes until a coherent final result is obtained.

The contributions of this paper are summarized as follows :

- We propose a synergistic cycle in which the three tasks of vertebrae segmentation, localization and identification cooperate and complement each other.
- We define a consistency criterion for the spine that

*. Corresponding author :

Email address: di.meng@inria.fr (Di Meng)

1. https://gitlab.inria.fr/spine/vertebrae_segmentation

is based on learned spine statistics of the vertebrae shape and of distances between the vertebrae. This enables a parameter-free approach to detect missing locations.

- We propose a location-segmentation refinement scheme that is able to achieve stable and accurate results. Additionally, it allows to merge duplicate locations with a parameter-free approach.
- We extend the work on individual vertebra classification (Mohammed et al., 2020) and show significant improvement on vertebrae classification by including neighboring information. We experimentally quantify that solely using the shape of the vertebrae achieves higher accuracy than using as input the CT image.
- We introduce a graph to enforce the global consistency of the predicted individual vertebrae labels. It allows to handle anatomically rare cases, e.g. the transitional vertebrae T13, L6 and the absence of T12.

The contributions of the paper are validated on the reference benchmarked VerSe20 challenge dataset (Sekuboyina et al., 2021) where the proposed method outperforms the state of the art approaches.

2. Related work

We start by reviewing the vertebrae labelling literature, addressing the localization and identification task. Then we review the multi-label segmentation methods which in addition handles the vertebrae segmentation.

2.1. Vertebrae labelling

For vertebrae localization and identification, traditional methods build on shape models (Cai et al., 2015; Lindner et al., 2014) or graphical models (Glocker et al., 2012; Bromiley et al., 2016) to detect landmarks. Such models are powerful since they encode prior knowledge about the full structure of the spine. In (Glocker et al., 2012) vertebrae locations are regressed by making assumptions on the shape appearance, but the approach is not robust to pathological cases or abnormal images with surgical implants. They further improve the method by transforming the sparse location annotation into dense labels in the surrounding area, which avoids modeling the vertebra shape (Glocker et al., 2013). Both approaches (Glocker et al., 2012, 2013) use random forests. Chen et al. (2015) share a similar idea and localize the coarse vertebrae candidates by training a binary RF classifier based on HOG features.

More recent methods build on machine learning and convolutional neural networks (CNN) in which hand-crafted features tend to be replaced by learned ones. Sekuboyina et al. (2018) combine information across several 2D projections using a butterfly-like architecture and encode the local spine structure as an anatomic prior with an energy-based adversarial training. Liao et al. (2018) and

Qin et al. (2020) develop a multi-label classification and localization network using FCN and residual blocks. They improve the classification branch with bidirectional recurrent neural network (Bi-RNN) to encode short and long range spatial and contextual information. In (Wang et al., 2021) a nnUnet keypoint detection model is trained to estimate 26 vertebrae activation maps. Chen et al. (2019) propose a variant FCN that localizes vertebrae in original resolution and classifies them in down-sampled resolutions. These are stand-alone networks that directly output vertebrae locations and identifications and can be trained in an end-to-end manner. However, these methods struggle to handle rare cases (missing T12 or occurrence of T13 or L6) as the anatomic consistency is not explicitly enforced. In addition, the scarcity of data with rare cases makes the end-to-end learning approaches under-perform in their detection.

Other works in the literature perform vertebrae labelling in multiple stages. McCouat and Glocker (2019) employ separate CNNs to localize the vertebrae in 3D samples and identify them in 2D slices with a two-stage method. In order to find vertebrae, Jakubicek et al. (2020) detect first the spine and then track the spinal cord based on the combination of a CNN and a growing sphere method. Payer et al. (2020) follow a similar strategy of coarse to fine vertebrae localization by detecting the spine in lower resolutions and each vertebra in higher resolution images. For identifying vertebrae, Chen et al. (2015) propose a joint learning model (J-CNN) that can classify the vertebrae labels and encode the pairwise conditional dependency at the same time. In our work, we also use multiple stages to obtain the vertebrae locations and identifications. In addition, we loop through a consistency check in order to enforce mutual consistency.

Since raw predictions from networks are not always accurate, various post-processing stages have been adopted to constraint vertebrae locations based on the anatomical ordering. Chen et al. (2015) use a shape regression model to correct the offsets from the deviation in the vertical axis. The model assumes that the coordinates distribution can be described by a quadratic form and is limited to coordinates on the vertical axis. Yang et al. (2017) introduce a chain-structure graphical model to depict the spatial relationship between vertebrae and regularize their locations with an L_1 norm to learn the best sparse representation. Chen et al. (2019) model the score maps interpolated along the 1-D spinal curve with a Hidden Markov Model to generate the optimized 1-D coordinates. In our approach, we propose an efficient graph that enforces inter-vertebrae constraints over the individual vertebra classification predictions, with the ability to model patients with or without transitional vertebrae.

2.2. Multi-label vertebrae segmentation

For the segmentation task, earlier methods mainly used statistical models (Klinder et al., 2009; Rasoulian et al.,

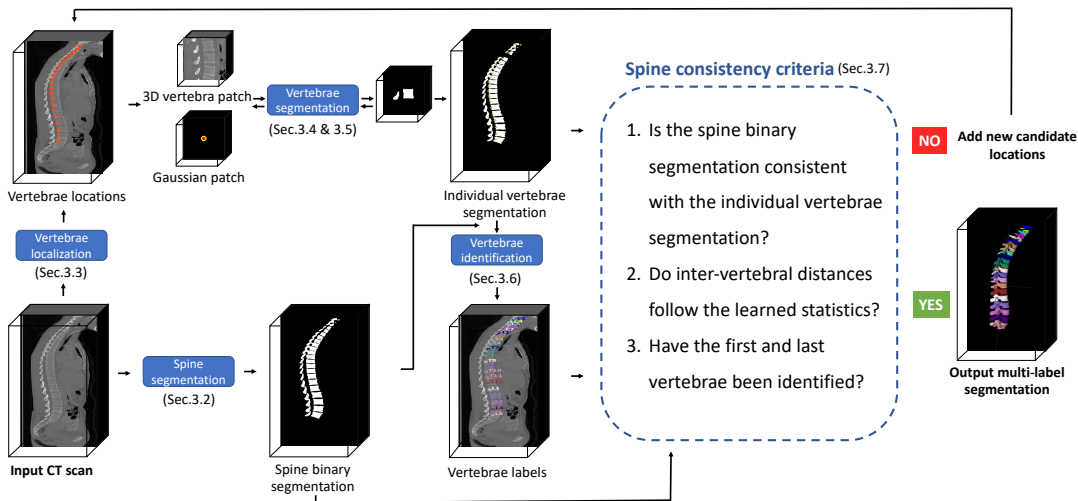


FIGURE 1: Overview of the proposed method. Starting with an input CT scan (bottom left) a binary segmentation is extracted. Vertebrae locations are then detected from the input CT. From each location an individual vertebra segmentation is extracted. Each location and individual vertebra segmentation is refined until convergence. This refinement allows to detect and remove duplicated locations. Using the union of the spine binary segmentation and the individual segmentations, the vertebrae are identified using a two step local and global approach. At this point the current locations, identifications and segmentations are analyzed with a spine consistency check. If the spine consistency criterion is not satisfied then new candidate locations are added and the loop goes back to the location segmentation refinement step. If the consistency is reached, the method outputs the current result.

2013), active shape models (Graham et al., 1995; Benjeloun et al., 2011; Al Arif et al., 2016), graph cuts (Aslan et al., 2010), and level sets (Tsai et al., 2003; Lim et al., 2014). Recent learning based approaches have nevertheless demonstrated better performances. Al Arif et al. (2017) use a deep convolutional neural network for cervical vertebrae segmentation and introduce a shape-aware term in the loss function. The approach is semi-automatic and the vertebrae locations are given manually. Sekuboyina et al. (2017) propose a two-stage approach for lumbar vertebrae segmentation in which they first regress the bounding box of the lumbar region and then segment and label each vertebra locally. We follow a similar principle, by first computing vertebrae locations which are used as a support for the segmentation (Sec. 3.3). In a complementary way, we compute a binary segmentation of the full spine (Sec. 3.2) that is used as a strong support in our framework to locate missing vertebrae.

Several methods achieve very good performances by assuming that a specific part of the spine is observed (Janssens et al., 2018; Al Arif et al., 2018a,b). However, these methods are not robust to arbitrary field of views. Lessmann et al. (2019) handle this issue by iteratively applying convolutional networks in the CT images. The vertebrae are segmented and identified as they are progressively found with a sliding window. This method heavily relies on the first detection and hardly recovers from failures that occur during this first stage. To address this limitation, Altini et al. (2021) propose a semi-automatic method that requires the user to provide the identity of the first top vertebra and the total number of vertebrae.

Masuzawa et al. (2020) propose a multi-stage framework where, first, the bounding boxes of cervical, thoracic and lumbar vertebrae are found, then the vertebrae in each bounding box are segmented and identified in an iterative manner. This approach reduces the intra-class variance from identifying one out of 24 vertebrae into identifying one out of 7 cervical, 12 thoracic and 5 lumbar vertebrae. Similarly, Mohammed et al. (2020) quantify that a two-step approach has a higher identification rate. In our work we leverage this two step approach and extend the work of Mohammed et al. (2020) by including neighbouring vertebrae.

Payer et al. (2020) use a three-step approach to first localize the spine, then simultaneously locate and identify each vertebra and finally segment each individual vertebra. The segmentation, identification and localization of the vertebrae are performed with a chain of modules and when a vertebra is not located, it is not segmented. Kim et al. (2021) propose a very similar approach to detect and segment vertebrae in X-ray images. In our method we propose to cycle back through the modules until a coherent final result is met. This cycle allows us to recover from potential detection failures.

3. Method

3.1. Overview

The input to our method is a CT volume with an arbitrary field of view, resolution and anatomic position, potentially imaging a human spine. The CT volume is first pre-processed : it is re-sampled into an isotropic resolution

of $1 \times 1 \times 1 \text{mm}^3$ and re-oriented into a PIR anatomic orientation, where P stands for *towards the back of the body*, I for *towards the bottom of the body* and R for *radial aspect of the forearm*. In the following, when we mention the *input CT* we refer to the pre-processed data.

An illustration of the proposed framework is shown in Fig. 1. Our method first computes a binary segmentation mask of the spine (Sec. 3.2) and a set of initial 3D vertebrae locations (Sec. 3.3). From the 3D locations, individual vertebrae are segmented (Sec. 3.4), and their 3D locations refined until convergence (Sec. 3.5). This step allows to identify and discard duplicated locations. Next, the locations and individual masks are identified (Sec. 3.6). The current result composed of the vertebrae localization, identification and segmentation is then evaluated using a spine consistency criterion (Sec. 3.7). In the case of consistency, the result is validated and considered final. We output the segmentation in original resolution and orientation. Otherwise, new 3D vertebrae locations are added and the locations refinement (Sec. 3.5) and the identification (Sec. 3.6) are cycled through until a consistent solution is found. We next detail the individual components of the pipeline.

3.2. Binary spine segmentation

Computing a binary segmentation of the spine is an easier task than computing individual vertebrae segmentations. While the binary spine mask does not have the detailed information of each vertebra, in our work we will use it as a support to validate that the individual segmentations are consistent (Sec. 3.7).

Given the input CT, we compute a binary segmentation of the spine using an Attention U-net (Oktay et al., 2018). The backbone architecture is a 3D U-net (Ronneberger et al., 2015) with attention blocks embedded in the skip connections. The output of the network is a probability mask with floating values in range $[0, 1]$ for each voxel indicating if it belongs to the spine or not. As the input CT has an arbitrary size and the network accepts only a fixed sized input, we use patches of size $96 \times 96 \times 96$ as the input to our network.

To train the network we use a regression loss \mathbf{L} that combines the Dice coefficient and the Mean Squared Error, the objective being to minimize the difference between our prediction and the ground truth. In detail, denoting the input as x , the output as $G(x)$ and the ground truth patch as y , we define

$$\mathbf{L}(G(x), y) = \mathbb{E}_{x,y} \left[1 - \frac{2|G(x) \cdot y|}{|G(x)|^2 + |y|^2} \right] + \lambda \mathbb{E}_{x,y} [\|y - G(x)\|_2], \quad (1)$$

where λ was empirically set to 10 and kept constant in all our experiments.

At inference time, the model is applied in a sliding mode over the whole CT volume with a stride length of 24 (one quarter of the patch size) and for each voxel we obtain 64 predictions. We aggregate the results in each voxel by

averaging the 64 probability maps and binarize the result with a 0.5 threshold.

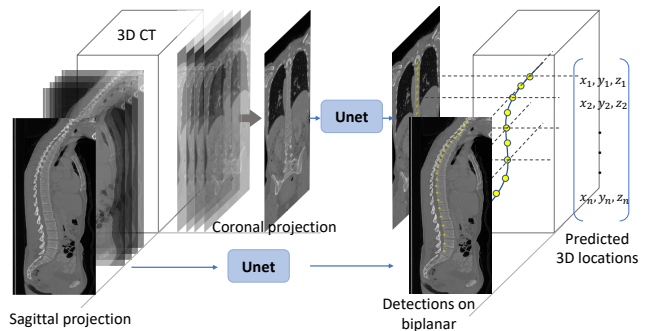


FIGURE 2: Vertebrae localization in a 3D CT image.

3.3. Initial vertebrae localization

The goal of this step is to obtain a first set of 3D locations. Instead of directly working on the 3D volume, we project it into the sagittal and coronal planes to obtain two orthogonal 2D views. Then 2D vertebrae locations are independently detected in both projections and 3D locations are reconstructed by matching each 2D location with its nearest neighbor.

The 2D vertebrae detection is performed using 2 U-nets (Ronneberger et al., 2015) on sagittal and coronal views respectively. The output is a 2D probability map where the vertebrae centroids present the highest probabilities in range $[0, 1]$. We use a Weighted Hausdorff Distance Loss (Ribera et al., 2019), minimizing the maximal distances between the predicted and ground truth locations. From the obtained 2D locations on the bi-planar views, we cast rays along the coronal and sagittal axes. We then compute the 3D distances between the rays and use the nearest neighbor strategy to merge the 2D points into 3D locations. Matches with a distance higher than 10mm are discarded.

We would like to emphasize that the goal of this step is to obtain an initial set of 3D locations. At this point, locations might be missing or duplicated. Our framework is designed to recover from such errors.

3.4. Individual vertebra segmentation

The goal of this step is to obtain an individual vertebra segmentation for each detected vertebra location. We consider as input a crop of the input CT image centered at the given 3D vertebra location and follow a strategy similar to (Sekuboyina et al., 2021), where an auxiliary location channel is used. This location channel contains the 3D location converted into a 3D probability map using a Gaussian kernel with $\sigma = 20$. The output is a one-channel probability map which is then binarized with the threshold 0.5 to obtain the final binary mask. Different from (Sekuboyina et al., 2021) we use the Attention U-Net described in Sec 3.2 with an input cube size adapted to $128 \times 128 \times 128$

in order to cover any full shaped vertebra in *any orientation*. The individual vertebra segmentation network is trained by minimizing Eq. 1 with $\lambda = 20$. Although the input is in PIR orientation, some vertebrae, especially cervical, have important rotations around the Z-Axis. In addition, the input 3D locations might be not accurate. To make the network robust to these cases at inference time, we augment the training data with vertebrae locations translated with an offset $t \in [-10, +10]^3$ mm as well as vertebrae rotated by $[\min(-50, \theta - 50), \max(50, \theta + 50)]$ degrees around the Z-Axis, where θ is the vertebra rotation wrt the axial plane. The angle θ is computed using the current and next vertebrae locations. Each sample is augmented 162 times.

3.5. Vertebra location and segmentation refinement

From the initial locations we obtain individual segmentation masks. However, given an individual vertebra binary segmentation, the vertebra location can be approximated by computing the center of mass of the segmentation mask. This heuristic produces a fairly precise estimate, provided the quality of the segmentation mask is good enough, as we show in Sec. 4.5. Thus, from a given location, the segmentation is able to predict a single vertebra mask. Then, one can compute the new center of mass of the predicted segmentation and get a new location. In our work we study if this cycle can be iterated until an agreement of the location and the individual segmentation mask is reached. In Sec. 4.5 we present the results on the accuracy and the convergence of this iterative refinement.

3.6. Vertebrae Identification

As mentioned earlier, identifying vertebrae is a challenging task for several reasons, including their similar shapes. To address this challenge, we propose to combine a local and a global reasoning. For the local reasoning, we use an individual classification method predicting one of the 24 possible labels for each vertebra. At a larger scale, we use the prior knowledge that vertebrae are *sorted* in the spine and aggregate the local information into a global, consistent final identification.

3.6.1. Individual local classification

The individual vertebra identification module builds on the work by (Mohammed et al., 2020) where a 3D network is used to classify vertebra into one of their 24 categories. The input of the network is a binary volume of size $128 \times 128 \times 128$ that contains a vertebra segmentation mask. The output is the N dimensional vector of all class probabilities. The prediction proceeds in two stages. First, a group label, i.e., cervical, thoracic or lumbar vertebra, is predicted ($N = 3$). Second, the individual vertebra goes into a per group classifier to predict the identity within the group ($N = 7/12/5$). As shown in (Mohammed et al., 2020), the two-stage method obtained a higher accuracy than directly classifying into one of the 24 categories.

In the current work, we extend the method by adding the neighboring vertebrae segmentation masks to the input, while keeping the target vertebra in the center of the cube as shown in Fig. 3. The input to the classifier at inference time is the union of the binary segmentation of the spine (Sec. 3.2) and the individual vertebra segmentation (Sec. 3.4). In order to deal with pathological cases, such as T13 or L6, for which we only have a small number of samples in the training set - one T13 and thirteen L6 in practice - we consider T13 as T12 and L6 as L5 and leave their fine identification to the global reasoning. Quantitative results and comparison to the previous method are reported in Sec. 4.6.

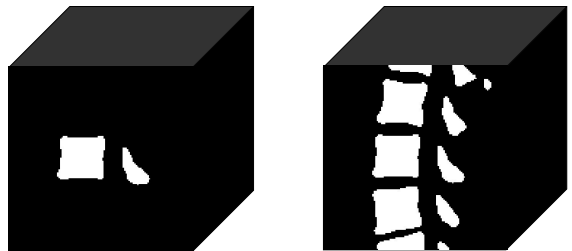


FIGURE 3: Input cube to the vertebrae classification network. Left : individual vertebra; Right : Individual vertebra with neighboring context.

3.6.2. Individual global identification

The local classification is not perfect and some vertebrae can be misidentified. However we propose to take advantage of a global approach to enforce the natural ordering of vertebrae, i.e. consecutive vertebrae should get consecutive labels. To enforce this global consistency we formulate the problem as a shortest path problem in a graph, as shown in Fig. 4. Given a list with n consecutive locations we create a graph with $n \times 24$ nodes. Each of the n columns represents a location, and each of the 24 rows represents a vertebra class. We formulate two types of cost, the unary and the binary costs. We populate the unary cost of each node with the cost obtained from the individual local probability, a value in the range $[0,1]$. Additionally, as the 3-group predictions are very reliable, we also add a cost to each unary to prevent group swapping. The binary costs are encoded in the edges of the graph. These edges between nodes encode the knowledge if two consecutive vertebrae have a consistent class or not, i.e., node N_i^j with $i \in [1, n]$ and $j \in [1, 24]$ is only connected with N_{i+1}^{j+1} . This effectively enforces that consecutive vertebrae get consecutive labels.

Three configurations need special attention. They correspond to non standard configurations : i. The presence of T13, ii. The lack of T12 and iii. The presence of L6. To handle the presence of T13, an edge is added between two consecutive T12 nodes, shown in blue in Fig. 4. For

the lack of T12, an edge is added between two consecutive nodes belonging to T11 and L1, shown in brown in Fig. 4. The presence of L6 is dealt with an edge between two consecutive L5 nodes, shown in blue in Fig. 4. These special edges are given a higher cost of 2. To complete the graph, two extra nodes with no cost are added to be used as the source (*src*) and the destination (*dst*) in the optimization. The *src* node is connected to all nodes of the first vertebrae and the *dst* node is connected to all nodes of the last vertebrae.

Once the graph is created and the costs are populated, we compute the shortest path in the graph using the classical Dijkstra algorithm (Dijkstra et al., 1959). As a post process, we check if repeated instances of T12 (or L5) are obtained and adjust the class of the second node to T13 (or L6) accordingly.

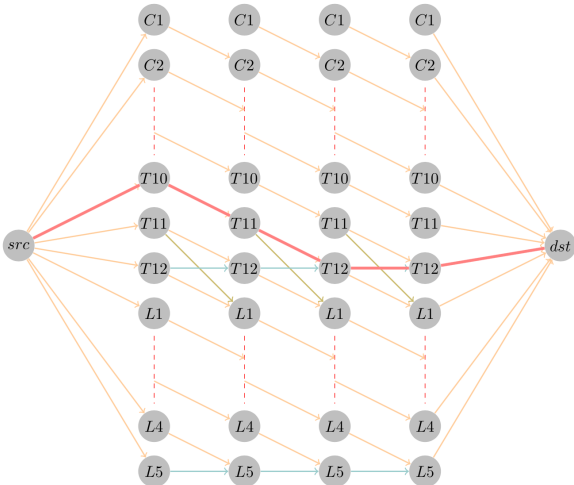


FIGURE 4: Spine identification global graph. Example with 4 vertebrae. Edges in orange are regular connections between nodes. Edges in blue connecting T12 to T12 (and L5 to L5) allow for the presence of T13 (and L6). The edge between T11 and L1 allows for T12 to be absent. The result with red edges corresponds to a spine where T10, T11, T12 and T13 are observed. (Best viewed in color)

3.7. Spine consistency criteria

Once we have identified all vertebrae, we have a set of consistent locations and segmentation masks, as well as a consistent identification for each of the detected vertebrae. We need to consider if they can formulate a coherent output. Owing to the fact that, if a location was missed in the first step (Sec. 3.3), not only we would be missing it, but as a consequence, the *consistent* identifications would be wrong. In order to detect missing vertebrae and output a coherent segmentation, we propose three spine consistency criteria. Each of the criteria will not only allow us to detect if a vertebra is missing, it will also allow to add new candidate vertebrae locations. The new locations will be either consistently refined into a new location (Sec. 3.5) and kept, or merged into an existing location and then discarded. If new refined locations are added, the identification

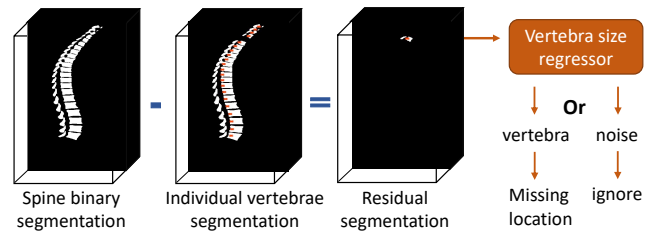


FIGURE 5: Spine consistency criterion : Inconsistencies between the individual vertebrae segmentations and the spine binary segmentation can identify missing vertebra.

is re-computed (Sec. 3.6) and the three spine consistency criteria checked again. The process is stopped when all three spine consistency criteria are met, or the set of locations, identifications and segmentation masks does not change over one loop. We next detail the three proposed spine consistency criteria.

The first criterion is that the union of all individual vertebrae should be consistent with the spine binary segmentation. To check this criterion, the union of the individual masks is subtracted from the spine segmentation and the residual connected components is obtained. These components correspond either to missing vertebrae or segmentation noise. In the human spine, the size of consecutive vertebrae is heavily related, thus we propose to use the size of these components to decide if a component is a missing vertebra, or noise. More specifically, linear regressors are trained to predict the size of the neighboring vertebra from the previous (and the next) one. The learned coefficients are provided in the Appendix A. As the individual identification might be wrong, especially if a vertebra is missing, we rely on the anatomic group identification. Two regressors (from previous and next) are trained for each anatomic group (cervical, thoracic and lumbar). When a residual is found, the nearest segmented vertebra is found. Its identification and the signed distance determines which regressor (previous or next) to use. If the residual’s size is larger than 50% of the predicted size, we consider it a vertebra and a new location at the center of the residual is added. If the residual’s size is smaller, it is considered as noise and discarded. Let us note, that using a fixed threshold on the size of the residual to decide if it is a vertebra does not work, as different vertebrae have varying sizes, for instance lumbar vertebrae can be three times larger than cervical vertebrae.

In our second criterion, we consider the case where the binary mask is not perfect, and some vertebrae are still missed (Sec. 4.2). To identify this case we leverage the fact that distances between locations are well structured in the spine. We propose to learn two statistical models of the distance between vertebrae. The first is a Gaussian distribution of the vertebrae distances for each anatomic group. The second are linear regressors predicting the vertebrae distance from its context. Effectively we learn to

predict the distance between vertebrae from the distance between the previous vertebrae, the distance between the next ones or using both side distances. These regressors are specific for each anatomic group and the learned coefficients are provided in the Appendix A. If a distance is larger than the predicted distance, we add an additional location in the middle of this gap and we loop again through the pipeline.

Our third and last criterion is that either C1 (and L5) should be identified or the top (or the bottom) of the volume should be reached. Effectively, if C1 (or L5) is not found at the spine extremity, an additional location is predicted up (or down) using the two most top (most down) locations. If the predicted location is inside the volume, it is added and the pipeline gets iterated once more. If the predicted location is outside the volume, the criterion is considered fulfilled.

4. Experiments

In this section we first introduce the dataset used for the main evaluation and for the comparison with the state of the art (Sec. 4.1). We then present the individual evaluations of the different modules that compose our method : the binary spine segmentation (Sec. 4.2), the initial vertebrae locator (Sec. 4.3), the individual vertebra segmentation (Sec. 4.4), the stability of the location-segmentation refinement (Sec. 4.5) and the vertebrae identification (Sec. 4.6). Finally we report on the full pipeline results (Sec. 4.7) and on an ablation study that demonstrates the respective benefits of the different modules (Sec. 4.8). Additionally, we show the results of our method on other challenging spine datasets which allow us to discuss its current limitations (Sec. 4.9).

4.1. Dataset

To evaluate our method we used the dataset from the VerSe20 MICCAI challenge (Löffler et al., 2020; Sekuboyina et al., 2020, 2021), which is currently the biggest such dataset on spine. It is split into a public training set, a public testset and a hidden testset. Each set consists of 100 CT images. We used the training set data and the associated annotations to set up our method. 80 random CT scans from the training set were used for training the networks and the rest (20) were used for validation. For the evaluation of each individual module we used the public testset and for the comparison with the state of the art we evaluated on both the public and hidden test sets.

Figure 6 shows an overview of the public training set structure. Each column represents a scan of a patient, and each row represents the presence of one of the 26 vertebrae, from C1 to L6. The arbitrary field of view of the input images can be observed, in that each scan covers often a few vertebrae only. The data is class imbalanced : more thoracic and lumbar vertebrae are present in comparison to fewer cervical vertebrae. Let us note that atypical

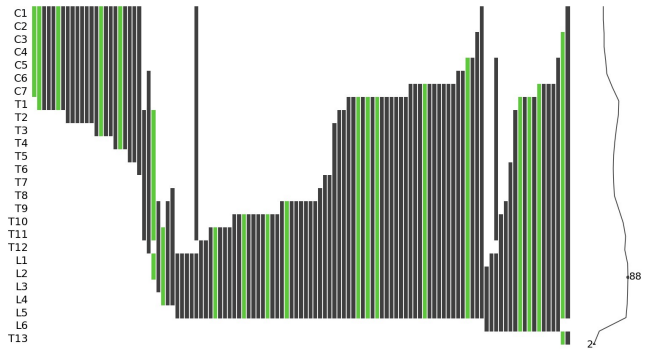


FIGURE 6: Dataset coverage (VerSe20 challenge public training set). Gray : our training set ; Green : our validation set. Each column represents a scan of a patient, and each row represents the presence of one of the 26 vertebrae, from C1 to L6. On the right the aggregated number of vertebrae is shown. (Best viewed in color)

anatomies are present in this dataset : in the transitional vertebrae there are cases with occurrences of T13 or absence of T12, as well as some occurrences of L6 cases.

4.2. Binary spine segmentation

The binary segmentation is used in the individual identification step (Sec. 3.6) as well as in spine consistency criteria (Sec. 3.7). Optimally, the spine binary segmentation should be the sum of all the individual vertebrae masks. To evaluate the general coverage of the spine by the binary spine segmentation, we use the Dice coefficient (DSC) and Hausdorff Distance (HD) metrics. As shown in Table 1, we achieve a mean Dice score of 94.51% and a mean HD error of 26.14mm. To evaluate if the binary segmentation of the spine covers each individual vertebra and how much they overlap, we use a pseudo Dice score

$$pseudo_dsc = \frac{2 \times G_i \cdot (G_i \cap P_s)}{G_i^2 + (G_i \cap P_s)^2}, \quad (2)$$

where G_i is the ground truth binary mask of individual vertebrae and P_s is our predicted binary mask of the spine. Since the spine segmentation is united and there's no vertebrae boundary information. The pseudo Dice score indicates how much GT individual vertebra is covered by our predicted spine segmentation. Instead of using the prediction of each vertebra which is here not available, we use the intersection of our spine binary segmentation with the vertebrae ground truth mask. Thus, we can quantify which part of each vertebra is covered by our predicted spine binary mask.

	DSC (%)		HD (mm)	
	mean±std	median	mean±std	median
public	94.51 ± 2.75	95.38	26.14 ± 22.84	23.34
hidden	94.34 ± 3.00	95.44	26.99 ± 16.16	22.82

TABLE 1: Evaluation of the spine binary segmentation.

		precision	recall	f-score	AHD
public testset	r=5	58.08	59.41	58.48	13.73
	r=10	85.16	87.88	85.99	
	r=15	90.87	94.35	92.04	
	r=20	91.93	96.06	93.46	
hidden testset	r=5	54.42	55.48	54.47	14.55
	r=10	80.88	83.69	81.43	
	r=15	87.64	91.26	88.49	
	r=20	89.88	94.11	91.04	

TABLE 2: Evaluation of the initial vertebrae locations.

In the public testset we observe that 94.65% vertebrae (1292 out of 1365) have a pseudo Dice score over 95%; 98.68% vertebrae (1347 out of 1365) have a pseudo Dice score over 80% and 99.78% vertebrae (1362 out of 1365) have a pseudo Dice score over 50%. Only one vertebra has a pseudo Dice below 40% (19.49%). In the hidden testset, 93.84% vertebrae (1264 out of 1347) have a pseudo Dice score over 95%; 99.33% vertebrae (1338 out of 1347) have a pseudo Dice score over 80% and 99.55% vertebrae (1341 out of 1347) have a pseudo Dice score over 50%; Five vertebrae having pseudo Dice below 40%. These results show that while the predicted binary spine segmentation faithfully segments most of the vertebrae, a few single vertebrae can still be missed. This advocates for a consistency criterion independent of the binary spine segmentation.

4.3. Initial vertebrae localization

For the initial vertebrae location evaluation, we report Precision(%), Recall(%), F-score(%) and averaged Hausdorff distance (AHD)(mm) (Ribera et al., 2019). A true positive is counted if there’s an estimated location at most at distance $r \in \mathbb{R}$ from a ground truth location. A false positive is counted if an estimated location does not have any ground truth location at a distance at most r . A false negative is counted if a true location does not have any estimated location at a distance at most r . Precision is the proportion of the estimated locations that are close enough to a true location. Recall is the proportion of true locations being detected. F-score is the harmonic mean of precision and recall. We report the evaluation with r in 5mm, 10mm, 15mm and 20mm in Table 2. In the results we observe that relatively few vertebrae have a very precise location (under 5mm). This result argues for a location refinement step. Similarly, several locations are still missed within a 20mm radius, motivating the need for a missing location recovery step.

4.4. Individual vertebra segmentation

We evaluated our individual vertebra segmentations using the Dice coefficient. Following Mohammed et al. (2020) results, we also explored whether the identification could help in the segmentation task, i.e. do specialized segmentation networks present higher accuracies than a *generic* one? We trained a *generic* network and three

anatomic-group-dedicated networks and compared them quantitatively. In Table 3 and Fig. 7 we present the obtained results. It is worth noting that the generic network outperforms the group specialized network, especially for the cervical vertebrae segmentation (Tab. 3). In addition, the generic segmentor exhibits less outliers than the specialized ones (Fig. 7) making the full pipeline less prone to missed vertebrae.

	group specialized		generic	
	DSC(%)	HD(mm)	DSC(%)	HD(mm)
cervical	88.99±6.11	13.78	93.02±3.03	6.18
thoracic	95.24±3.26	6.71	95.85±1.90	4.42
lumbar	96.11±5.02	8.10	96.66±4.36	5.65
overall	94.76±4.81	8.00	95.76±3.21	5.02

TABLE 3: Evaluation of the generic and specialized segmentors.

4.5. Stability study of the location and segmentation refinement

One key element of the proposed pipeline is the location and segmentation refinement (Sec. 3.5). First we quantify the accuracy of the heuristic that is used when computing the location of a vertebra as the center of mass of the segmentation mask. For every GT vertebra mask in the training set, we computed its gravity center. We then computed the Euclidean distance between each gravity center and its GT location and obtained a mean distance error of 0.67mm. We consider this sub-pixel precision accurate enough to validate the approach.

Next we study the convergence of the refinement process : we initialize a location with a perturbation from the GT, run the iterative refinement and observe the result. We initialized the location with different initial settings : GT, GT+5mm, GT+10mm and GT+15mm. For GT, the converged locations end up with 1.19mm mean distance error and converged masks achieve 91.43% DSC. For the perturbation of 5mm, 10mm and 15mm, the converged location errors are 1.22mm, 1.21mm, 1.21mm and the converged masks obtain a Dice score with 91.37%, 91.67%, 91.62% accuracy respectively. In Fig. 8 we show for the case of GT+15mm how the distances between the locations of

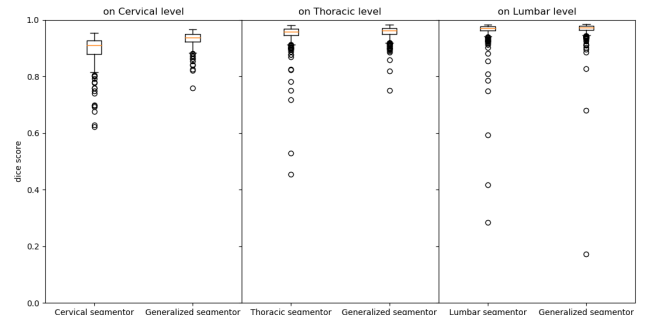


FIGURE 7: Boxplots of Dice score : generic segmentor vs specialized segmentors.

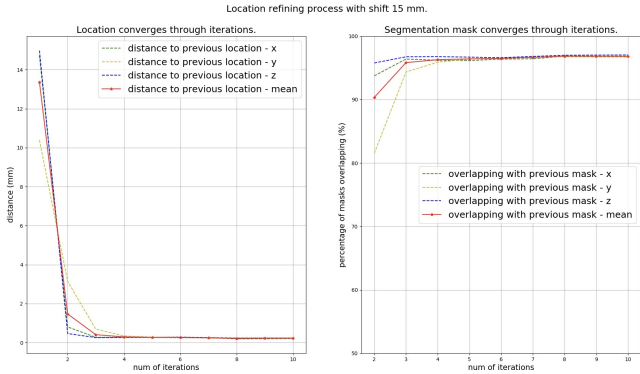


FIGURE 8: Vertebrae location-segmentation refinement. X axis represents the number of iterations. Left : locations convergence. Y axis represents the Euclidean distance to the previous locations. Right : segmentation convergence. Y represents the percentage of the overlapping with the previous segmentation mask.

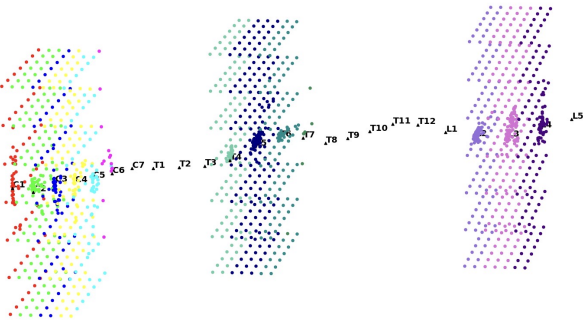


FIGURE 9: Basin of attraction of the vertebra location. We show the initial locations sampled around C3, T5 and L3, their converging waypoints and converged locations. (Best viewed in color)

consecutive iterations get smaller (left), and how the overlap of consecutive segmentation masks becomes stable (right).

To better understand the *bassin of attraction* of each vertebra we perform an experiment where we sampled initial locations on a 60mm cube grid around a GT location with a stride of 10mm. In Fig. 9 we present the visuals for three vertebrae. Each vertebra is associated with one color and we color-code each initial location with the color of the vertebra to which the refinement converged. For instance, red represents C1 and red dots mark the initial locations that converged to the C1 vertebra. We note how the initial locations color coding is structured in space, neighbouring initial locations converged either to the same vertebra, or the neighbouring one. It is also worth noting that the size of the *bassin of attraction* differs for cervical, thoracic and lumbar vertebrae. Its size is clearly related to the size of the vertebrae; the thoracic and lumbar vertebrae have a larger size than the cervical ones.

4.6. Vertebrae identification

As presented in Sec. 3.6.1 we extended the method of Mohammed et al. (2020) by considering the context of the neighbouring vertebrae. With this approach we obtain an accuracy of 84.55%, which represents an improvement of 14.05% with respect to the single vertebra approach. In Appendix B we provide the obtained confusion matrix. It is worth noting that the thoracic and lumbar vertebrae are the ones with most confusions and the most common confusion is a prediction of the next or previous vertebra.

To evaluate the benefit of the proposed global individual identification (Sec. 3.6.2) we performed the graph optimization with the obtained predictions from the local identification. The identification accuracy is improved from 84.55% to **97.36%**. As the output of the graph is always a consistent spine, the only failures are the ones caused by a label shift.

	Group	Cervical	Thoracic	Lumbar	Individual
w/o	99.48%	82.32%	67.44%	72.85%	70.50%
w/	99.56%	96.95%	83.25%	79.63%	84.55%

TABLE 4: Individual vertebrae classification accuracy with and without context.

4.7. VERSE Challenge

We quantitatively evaluated our method on the VerSe 2020 Challenge public and hidden testsets with 200 CT subjects in total and adopted the metrics of the challenge evaluation protocol (Sekuboyina et al., 2021). The *Dice coefficient (DSC)* : a variant of intersection over union to asses the similarity of two segmentations. The *Hausdorff Distance (HD)* : the Hausdorff distance between two segmentation surfaces. The *Mean Localization Distance (MLD)* measuring the Euclidean distance of the predicted location to the GT location. The *Identification rate (ID rate)* : a predicted location within 20mm from the GT location is considered as a valid identification and the ID rate is the ratio of valid identifications over all present vertebrae. The DSC and HD evaluate the segmentation performance while the ID rate and MLD evaluate the accuracy of the labeling task. Table 6 shows the results of the proposed method and the top scoring methods in the benchmark. Our method is on pair with the best performing method in the leaderboard (Chen et al., 2020).

It is worth noting that the method by Chen et al. (2020) did not win the challenge, as one important cri-

methods	DSC - public	DSC - hidden
ours	88.56%	91.48%
Payer C.	85.96%	89.59%
Zhang A.	87.15%	87.35%
Chen D.	84.21%	87.01%
Yeah T.	87.04%	82.07%

TABLE 5: Pipeline evaluation on anatomically rare cases. (Sekuboyina et al., 2021)

terion in the challenge was the performance in handling the anatomically rare cases - 6 cases with T13 (2/2/2 in Train/Public/Hidden), 47 cases with L6 (15/15/17) and 8 cases with absent T12(3/4/1). Following the challenge guidelines we computed the Dice score only on these scans and the obtained results are presented in Table 5. Our method clearly outperforms all the state of the art methods in handling the anatomically rare cases.

4.8. Ablation study

In this work, we propose a synergistic cycle where the three tasks - vertebrae localization, identification and segmentation help and complement each other. The missing locations can be recovered and a stable and consistent multi-label segmentation can be obtained. To assess the benefits of the synergistic cycle explained in Sec. 3.7, we performed an ablation study of the proposed pipeline by removing it (Tab. 7 i). To assess how sensitive our pipeline is to the input initial locations and binary spine segmentation, we performed two experiments. In the first we started with zero initial locations (Tab. 7 ii) and explored how well the synergistic cycle can recover. In the second we used an empty binary spine segmentation as input to the synergistic cycle (Tab. 7 iii).

Table 7 shows that, by removing the synergistic cycle from the pipeline, the accuracy drops 14.03% for DSC and 19.33% for ID rate. The errors are accumulated and propagated through the sequential pipeline. The proposed synergy loop effectively allows to recover mistakes. Starting with zero initial locations is an extreme scenario. However, the proposed method is capable to find the missing locations. The binary segmentation, together with the consistency criteria are able to recover most locations one by one. Using an empty binary spine segmentation tests the contribution of its accuracy to the final pipeline. The results in Table 7 iii show that the spine consistency check based on the statistics performs well and allows to recover missed vertebrae. While the binary spine segmentation is a powerful component in finding missing locations, the proposed method still performs well without it.

	DSC(%)	ID rate(%)	MLD(mm)	HD(mm)
proposed	93.22	96.53	2.15	6.82
i	79.19	77.20	9.50	17.73
ii	89.79	92.45	3.47	8.88
iii	93.33	95.56	3.08	9.57

TABLE 7: Ablation study of the proposed pipeline. i) no synergistic cycle ; ii) zero initial locations ; iii) empty binary spine segmentation.

4.9. Other spine data

To further evaluate our method and examine its limitations and generalization capabilities we performed three additional evaluations. First we used a lumbar specific vertebrae dataset, then we used the xVertSeg dataset which has a specific focus on vertebrae fractures and we tested on a proprietary dataset where patients had a contrast

agent injected. The evaluated model is solely trained on the VerSe20 public training set.

Lumbar vertebra segmentation CT image database. The database (Ibragimov et al., 2014) consists of 10 CT lumbar spine images of 10 healthy subjects, each containing 5 lumbar vertebrae (i.e. levels from L1 to L5). For each vertebra, a reference manual segmentation is provided in the form of a binary mask. We took the 10 CT images as input and output a multi-label segmentation for each subject. As only the ground truth segmentation is provided, we quantitatively evaluated the Dice score. We get DSC (%) of 90.95 ± 0.79 and HD (mm) of 7.50 ± 1.00 , a consistent performance with the VerSe dataset. Qualitative visualizations can be found in Fig. 12.

xVertSeg database- Segmentation and Classification of Fractured Vertebrae. The xVertSeg.v1 database (Ibragimov et al., 2017) contains 25 CT lumbar spine images including non-fractured vertebrae and vertebrae with fractures of different morphological grades and cases. Among the 25 cases, 15 have a reference vertebra segmentation mask and fracture classification, while for the other 10 no annotations are publicly provided. We evaluated our method on the 15 images with ground truth annotations. For the quantitative evaluation, we obtain a mean Dice score of 46.19%. Only 5 out of 15 segmentations achieve a Dice score over 90%. The main failure of our method comes from the inability to segment fractured vertebrae. As our model is trained on VerSe20, which includes very few fractured vertebrae, the trained network does not generalize well to fractured ones. In future work will explore how to make the proposed model robust to fractures.

CT images with contrast agents. Next we tested our method on two CT images of patients who had contrast agents injected in the spinal cord. For both patients a reference was manually segmented by a technician. We obtain a Dice score (%) of 85.88 ± 3.11 , 91.05 ± 1.68 respectively and a HD error (mm) of 7.33 ± 2.01 and 6.30 ± 2.69 . When visually inspecting the obtained segmentations, we observe that our method is not robust to the contrast agents. The spinal foramen is not properly segmented as illustrated in Fig. 10 : the brightness created by the contrast agent is segmented as bone. In future work we will explore leads on how to overcome this limitation.

5. Discussion

In this work we propose a synergistic cycle for the three tasks - vertebrae segmentation, localization and identification, aiming to achieve a consistency through all blocks. We argue and quantitatively asses that the input of a task is potentially beneficial to improve another one, e.g. missing locations can be recovered and duplicated locations fused with a parameter free method. We next discuss how

methods	public testset				hidden testset			
	ID rate(%) \uparrow	MLD(mm) \downarrow	DSC(%) \uparrow	HD(mm) \downarrow	ID rate(%) \uparrow	MLD(mm) \downarrow	DSC(%) \uparrow	HD(mm) \downarrow
ours	96.53	2.15	93.22	6.82	94.97	2.46	91.51	6.83
Chen D.	95.61	1.98	91.72	6.14	96.58	1.38	91.23	7.15
Payer C.	95.06	2.90	91.65	5.80	92.82	2.91	89.71	6.06
Zhang A.	94.93	2.99	88.82	7.62	96.22	2.59	89.36	7.92
Yeah T.	94.97	2.92	88.88	9.57	94.65	2.93	87.91	8.41
Zeng C.	91.47	4.18	83.99	9.58	92.82	5.16	84.39	8.73

TABLE 6: Pipeline evaluation on VerSe20 MICCAI challenge benchmark. We only report the scores. For the final ranking, ID rate and Dice are weighted twice than MLD and HD. Hidden testset has twice weight as Public testset. The segmentation task has twice weight of the labelling task. Transitional vertebrae detection is given more weight. More details about the position computing can be found in Sekuboyina et al. (2021).

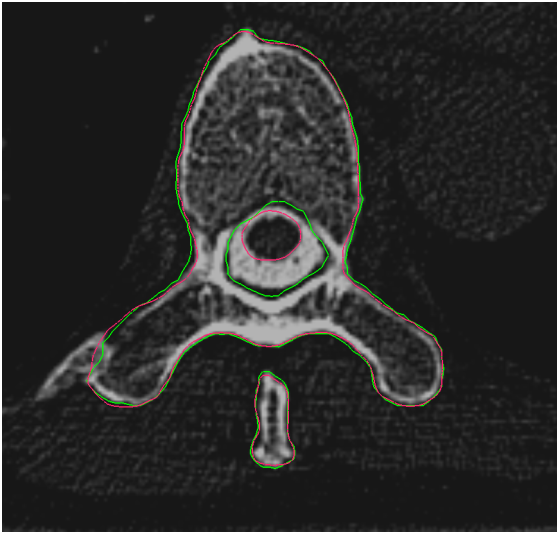


FIGURE 10: Segmentation of the spinal cord contrast agent. GT in green; Our prediction in red. Our method over-segment the contrast agent as bone.

the components in the synergistic cycle help and complement each other.

How does location help segmentation? The locations are used as anchor points for the individual segmentation module (Sec. 3.4). We experimentally tested to segment vertebrae without the location anchor and obtained lower performance.

How does segmentation help location? The location can be refined as it can be computed as the mass center of the segmentation mask. Moreover, as presented in Sec. 3.5, their iterative refinement converges to a stable pair of location and segmentation mask.

How does segmentation help identification? Our individual classification module (Sec. 3.6) takes as input an individual segmentation mask and predicts the identity of the vertebra. We experimentally tested to identify the vertebrae directly from the CT images and obtained lower performance.

How does location help identification? The locations of the vertebrae allow to sort the individual predictions for each individual vertebrae masks. This allows us to for-

mulate the shortest path optimization (Sec. 3.6.2) in a principal way. Moreover, as the location helps the segmentation and the segmentation helps the identification, the locations transitively help the identification task.

How does identification help location? Although there is no direct module extracting the location from the identification, identification plays a crucial role in detecting missing locations (Sec. 3.7). The per-anatomic-region adaptive size threshold takes advantage of the vertebrae identification to distinguish if the inconsistency between the binary and individual segmentation masks is a full missing vertebra or segmentation noise.

How does identification help segmentation? Identification helps segmentation in a transitive path through locations. In Sec. 4.4 we explored if per-anatomic class specialized networks could provide finer segmentations. However, Table 3 shows that the generic segmentation provided a higher accuracy. We hypothesize that this result is due to the relatively small amount of per-anatomic vertebrae and future work will elucidate if these results are consistent with more data.

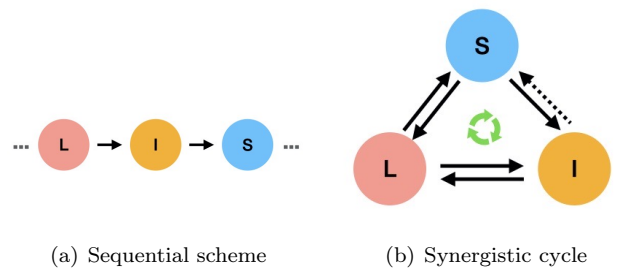


FIGURE 14: State of the art methods use a sequential scheme for localization, identification and segmentation of vertebrae. Our method leverages a synergy circle in which the output of a task can be used to improve another one until a consist results is reached.

6. Conclusion

In this paper we present a robust framework where the three tasks of vertebrae segmentation, localization and identification help and complement each other in a synergistic cycle. In contrast to existing state-of-the art methods

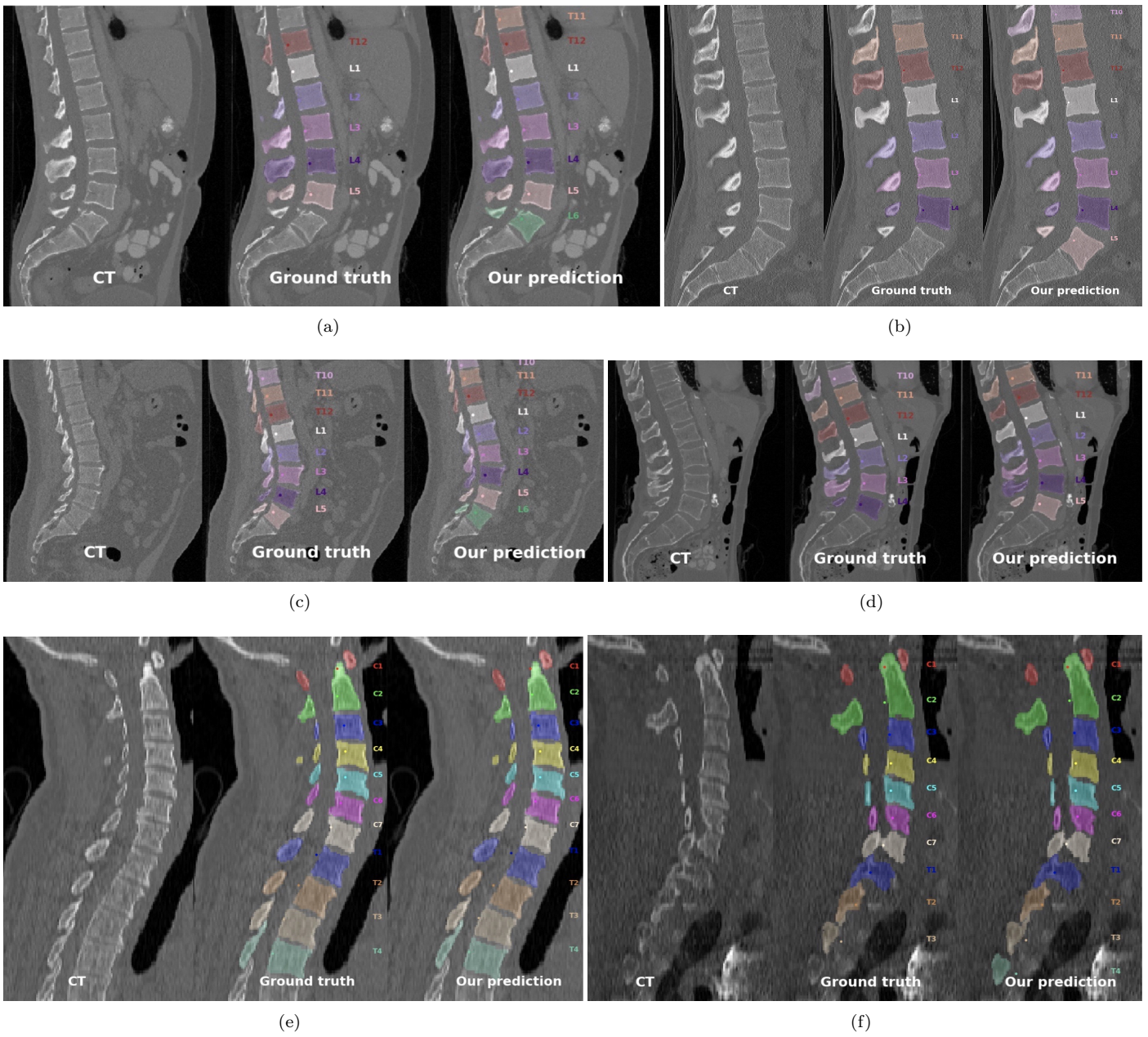


FIGURE 11: VerSe20 results visualization. (a) Best score in public testset (DSC : 98%); (b) Best score in hidden testset (DSC : 98%); (c) Worst score in public testset (DSC : 0.00%); (d) Worst score in hidden testset (DSC : 0.00%); (e)(f) Two examples of cervical vertebrae (DSC : 95.28%, 94.58%). Our method can segment more than the GT as seen in (a)(b). The bad performances (c)(d) come from the one-label shift issue.

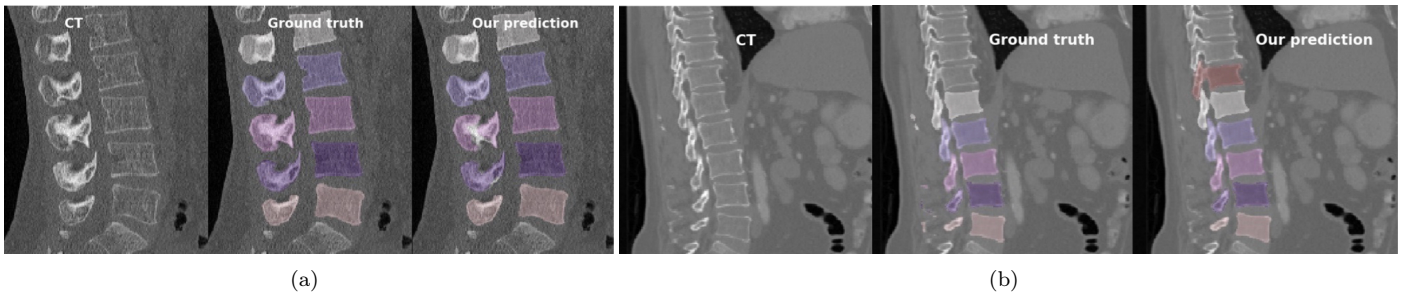


FIGURE 12: LumbarSeg dataset results visualization.(a) Best (DSC : 93.24%); (b) Worst (DSC : 90.25%).

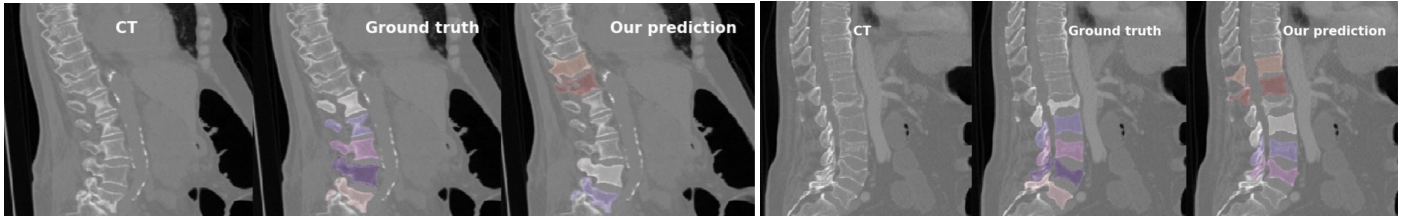


FIGURE 13: xVertSeg dataset failure results visualization. Our method collapses in the area of fractured vertebrae.

which treat the three tasks in a sequential process and each task is unable to recover from the mistakes of the previous module, we propose to cycle through the three tasks until a coherent result is reached. Our main contribution is the definition of the cycle through the localization, segmentation and identification tasks and the consistency criteria allowing to detect missing locations. We also contribute a segmentation-location refinement strategy, the extension of vertebrae identification by adding the context as well as a novel global graph optimization which is capable to handle anatomic rare cases with a simple approach. Our method outperforms the state-of-the-art algorithms on the verse20 challenge benchmark (Sekuboyina et al., 2021), particularly in the detection of transitional vertebrae. The models and code are made available for research purposes at https://gitlab.inria.fr/spine/vertebrae_segmentation.

We conducted further experiments that allowed us to identify the limitations of the proposed approach, namely the handling of fractured vertebrae and the artifacts created by contrast agents. Future work will explore leads to make our method robust to these cases.

Acknowledgments

This work was jointly supported by the Auvergne Rhône Alpes region, the Fonds Unique Interministériel [grant number 1701595901-N00013834] and the Grenoble Alpes metropole. The networks training in this work was performed using HPC resources from GENCI-IDRIS (Grant 2021-[AD011012208]). We thank Dr Kazu Hasegawa for the test dataset and the EOS imaging team for the manual expert segmentations used in the assessment.

Références

- Al Arif, S.M.R., Gundry, M., Knapp, K., Slabaugh, G., 2016. Improving an active shape model with random classification forest for segmentation of cervical vertebrae, in : International Workshop on Computational Methods and Clinical Applications for Spine Imaging, Springer. pp. 3–15.
- Al Arif, S.M.R., Knapp, K., Slabaugh, G., 2017. Shape-aware deep convolutional neural network for vertebrae segmentation, in : International Workshop on Computational Methods and Clinical Applications in Musculoskeletal Imaging, Springer. pp. 12–24.
- Al Arif, S.M.R., Knapp, K., Slabaugh, G., 2018a. Fully automatic cervical vertebrae segmentation framework for x-ray images. *Computer methods and programs in biomedicine* 157, 95–111.
- Al Arif, S.M.R., Knapp, K., Slabaugh, G., 2018b. Spnet : Shape prediction using a fully convolutional neural network, in : International Conference on Medical Image Computing and Computer-Assisted Intervention, Springer. pp. 430–439.
- Altini, N., De Giosa, G., Fragasso, N., Coscia, C., Sibilano, E., Prencipe, B., Hussain, S.M., Brunetti, A., Buongiorno, D., Guerriero, A., et al., 2021. Segmentation and identification of vertebrae in ct scans using cnn, k-means clustering and k-nn, in : Informatics, Multidisciplinary Digital Publishing Institute. p. 40.
- Aslan, M.S., Ali, A., Chen, D., Arnold, B., Farag, A.A., Xiang, P., 2010. 3d vertebrae segmentation using graph cuts with shape prior constraints, in : 2010 IEEE International Conference on Image Processing, IEEE. pp. 2193–2196.
- Benjelloun, M., Mahmoudi, S., Lecron, F., 2011. A framework of vertebra segmentation using the active shape model-based approach. *International Journal of Biomedical Imaging* 2011.
- Bromiley, P.A., Kariki, E.P., Adams, J.E., Cootes, T.F., 2016. Fully automatic localisation of vertebrae in ct images using random forest regression voting, in : International Workshop on Computational Methods and Clinical Applications for Spine Imaging, Springer. pp. 51–63.
- Cai, Y., Osman, S., Sharma, M., Landis, M., Li, S., 2015. Multi-modality vertebra recognition in arbitrary views using 3d deformable hierarchical model. *IEEE transactions on medical imaging* 34, 1676–1693.
- Chen, D., Bai, Y., Zhao, W., Ament, S., Gregoire, J., Gomes, C., 2020. Deep reasoning networks for unsupervised pattern de-mixing with constraint reasoning, in : International Conference on Machine Learning, PMLR. pp. 1500–1509.
- Chen, H., Shen, C., Qin, J., Ni, D., Shi, L., Cheng, J.C., Heng, P.A., 2015. Automatic localization and identification of vertebrae in spine ct via a joint learning model with deep neural networks, in : International conference on medical image computing and computer-assisted intervention, Springer. pp. 515–522.
- Chen, Y., Gao, Y., Li, K., Zhao, L., Zhao, J., 2019. vertebrae identification and localization utilizing fully convolutional networks and a hidden markov model. *IEEE transactions on medical imaging* 39, 387–399.
- Dijkstra, E.W., et al., 1959. A note on two problems in connexion with graphs. *Numerische mathematik* 1, 269–271.
- Forsberg, D., Lundström, C., Andersson, M., Vavruch, L., Tropp, H., Knutsson, H., 2013. Fully automatic measurements of axial vertebral rotation for assessment of spinal deformity in idiopathic scoliosis. *Physics in Medicine & Biology* 58, 1775.
- Glocker, B., Feulner, J., Criminisi, A., Haynor, D.R., Konukoglu, E., 2012. Automatic localization and identification of vertebrae in arbitrary field-of-view ct scans, in : International Conference on Medical Image Computing and Computer-Assisted Intervention, Springer. pp. 590–598.
- Glocker, B., Zikic, D., Konukoglu, E., Haynor, D.R., Criminisi, A., 2013. Vertebrae localization in pathological spine ct via dense classification from sparse annotations, in : International conference on medical image computing and computer-assisted intervention, Springer. pp. 262–270.
- Graham, J., Cooper, D., Taylor, C., Cootes, T., 1995. Active shape models their training and applications. *Computer Vision and Image Understanding* 61, 38–59.
- Ibragimov, B., Korez, R., Likar, B., Pernuš, F., Xing, L., Vrtovec,

- T., 2017. Segmentation of pathological structures by landmark-assisted deformable models. *IEEE transactions on medical imaging* 36, 1457–1469.
- Ibragimov, B., Likar, B., Pernuš, F., Vrtovec, T., 2014. Shape representation for efficient landmark-based segmentation in 3-d. *IEEE transactions on medical imaging* 33, 861–874.
- Jakubicek, R., Chmelik, J., Jan, J., Ourednicek, P., Lambert, L., Gavelli, G., 2020. Learning-based vertebra localization and labeling in 3d ct data of possibly incomplete and pathological spines. *Computer methods and programs in biomedicine* 183, 105081.
- Janssens, R., Zeng, G., Zheng, G., 2018. Fully automatic segmentation of lumbar vertebrae from ct images using cascaded 3d fully convolutional networks, in : 2018 IEEE 15th International Symposium on Biomedical Imaging (ISBI 2018), IEEE. pp. 893–897.
- Kim, K.C., Cho, H.C., Jang, T.J., Choi, J.M., Seo, J.K., 2021. Automatic detection and segmentation of lumbar vertebrae from x-ray images for compression fracture evaluation. *Computer Methods and Programs in Biomedicine* 200, 105833.
- Klinder, T., Ostermann, J., Ehm, M., Franz, A., Kneser, R., Lorenz, C., 2009. Automated model-based vertebra detection, identification, and segmentation in ct images. *Medical image analysis* 13, 471–482.
- Knez, D., Likar, B., Pernuš, F., Vrtovec, T., 2016. Computer-assisted screw size and insertion trajectory planning for pedicle screw placement surgery. *IEEE transactions on medical imaging* 35, 1420–1430.
- Lessmann, N., Van Ginneken, B., De Jong, P.A., Išgum, I., 2019. Iterative fully convolutional neural networks for automatic vertebra segmentation and identification. *Medical image analysis* 53, 142–155.
- Liao, H., Mesfin, A., Luo, J., 2018. Joint vertebrae identification and localization in spinal ct images by combining short-and long-range contextual information. *IEEE transactions on medical imaging* 37, 1266–1275.
- Lim, P.H., Bagci, U., Bai, L., 2014. A robust segmentation framework for spine trauma diagnosis, in : *Computational Methods and Clinical Applications for Spine Imaging*. Springer, pp. 25–33.
- Lindner, C., Bromiley, P.A., Ionita, M.C., Cootes, T.F., 2014. Robust and accurate shape model matching using random forest regression-voting. *IEEE transactions on pattern analysis and machine intelligence* 37, 1862–1874.
- Löffler, M.T., Sekuboyina, A., Jacob, A., Grau, A.L., Scharr, A., El Hussein, M., Kallweit, M., Zimmer, C., Baum, T., Kirschke, J.S., 2020. A vertebral segmentation dataset with fracture grading. *Radiology : Artificial Intelligence* 2, e190138.
- Masuzawa, N., Kitamura, Y., Nakamura, K., Iizuka, S., Simo-Serra, E., 2020. Automatic segmentation, localization, and identification of vertebrae in 3d ct images using cascaded convolutional neural networks, in : *International Conference on Medical Image Computing and Computer-Assisted Intervention*, Springer. pp. 681–690.
- McCouat, J., Glocker, B., 2019. Vertebrae detection and localization in ct with two-stage cnns and dense annotations. *arXiv preprint arXiv :1910.05911* .
- Merloz, P., Tonetti, J., Pittet, L., Coulomb, M., Lavallee, S., Troccaz, J., Cinquin, P., Sautot, P., 1998. Computer-assisted spine surgery. *Computer Aided Surgery : Official Journal of the International Society for Computer Aided Surgery (ISCAS)* 3, 297–305.
- Mohammed, E., Meng, D., Pujades, S., 2020. Morphology-based individual vertebrae classification, in : *International Workshop on Shape in Medical Imaging*, Springer. pp. 134–144.
- Oktaç, O., Schlemper, J., Folgoc, L.L., Lee, M., Heinrich, M., Misawa, K., Mori, K., McDonagh, S., Hammerla, N.Y., Kainz, B., et al., 2018. Attention u-net : Learning where to look for the pancreas. *arXiv preprint arXiv :1804.03999* .
- Payer, C., Stern, D., Bischof, H., Urschler, M., 2020. Coarse to fine vertebrae localization and segmentation with spatialconfiguration-net and u-net., in : *VISGRAPP (5 : VISAPP)*, pp. 124–133.
- Qin, C., Yao, D., Zhuang, H., Wang, H., Shi, Y., Song, Z., 2020. Residual block-based multi-label classification and localization network with integral regression for vertebrae labeling. *arXiv preprint arXiv :2001.00170* .
- Rasouliyan, A., Rohling, R., Abolmaesumi, P., 2013. Lumbar spine segmentation using a statistical multi-vertebrae anatomical shape+ pose model. *IEEE transactions on medical imaging* 32, 1890–1900.
- Ribera, J., Guera, D., Chen, Y., Delp, E.J., 2019. Locating objects without bounding boxes, in : *Proceedings of the IEEE Conference on Computer Vision and Pattern Recognition*, pp. 6479–6489.
- Ronneberger, O., Fischer, P., Brox, T., 2015. U-net : Convolutional networks for biomedical image segmentation, in : *International Conference on Medical image computing and computer-assisted intervention*, Springer. pp. 234–241.
- Sekuboyina, A., Hussein, M.E., Bayat, A., Löffler, M., Liebl, H., Li, H., Tetteh, G., Kukačka, J., Payer, C., Štern, D., et al., 2021. Verse : A vertebrae labelling and segmentation benchmark for multi-detector ct images. *Medical image analysis* 73, 102166.
- Sekuboyina, A., Rempfler, M., Kukačka, J., Tetteh, G., Valentinitch, A., Kirschke, J.S., Menze, B.H., 2018. Btrfly net : Vertebrae labelling with energy-based adversarial learning of local spine prior, in : *International Conference on Medical Image Computing and Computer-Assisted Intervention*, Springer. pp. 649–657.
- Sekuboyina, A., Rempfler, M., Valentinitch, A., Menze, B.H., Kirschke, J.S., 2020. Labeling vertebrae with two-dimensional reformations of multidetector ct images : An adversarial approach for incorporating prior knowledge of spine anatomy. *Radiology : Artificial Intelligence* 2, e190074.
- Sekuboyina, A., Valentinitch, A., Kirschke, J.S., Menze, B.H., 2017. A localisation-segmentation approach for multi-label annotation of lumbar vertebrae using deep nets. *arXiv preprint arXiv :1703.04347* .
- Tsai, A., Yezzi, A., Wells, W., Tempany, C., Tucker, D., Fan, A., Grimson, W.E., Willsky, A., 2003. A shape-based approach to the segmentation of medical imagery using level sets. *IEEE transactions on medical imaging* 22, 137–154.
- Wang, F., Zheng, K., Lu, L., Xiao, J., Wu, M., Miao, S., 2021. Automatic vertebra localization and identification in ct by spine rectification and anatomically-constrained optimization, in : *Proceedings of the IEEE/CVF Conference on Computer Vision and Pattern Recognition*, pp. 5280–5288.
- Yang, D., Xiong, T., Xu, D., Huang, Q., Liu, D., Zhou, S.K., Xu, Z., Park, J., Chen, M., Tran, T.D., et al., 2017. Automatic vertebra labeling in large-scale 3d ct using deep image-to-image network with message passing and sparsity regularization, in : *International conference on information processing in medical imaging*, Springer. pp. 633–644.

Appendix A. Vertebrae statistics

Vertebrae size regressor

To check if the spine binary mask and the vertebrae individual masks are consistent we subtract the union of the individual masks from the spine segmentation and compute the remaining residual connected components. These residuals may be a missing vertebrae or segmentation noise as binary and individual segmentations differ. We take advantage of the vertebrae identification to compute an adaptive threshold and use it discriminate between noise or a missing vertebrae.

To define if the residual is a missing vertebra or not, we analyze its size by learning linear regressors that predict the size of a vertebra from the size of the neighbor vertebra. We learn two types of regressors, one predicting the vertebra size from the previous vertebra size and one predicting the vertebra size from the next vertebra size. We train two linear regressors for each level of the spine (cervical, thoracic and lumbar) : $S_i = a * S_{i-1} + c_1$ and $S_i = b * S_{i+1} + c_2$,

and we use the corresponding depending on the current identification of the neighboring vertebrae. The learned coefficients are $(a = 1.03, c_1 = 1471, b = 0.92, c_2 = 497)$ for cervical, $(a = 1.03, c_1 = 1354, b = 0.94, c_2 = -140)$ for thoracic and $(a = 1.05, c_1 = 981, b = 0.94, c_2 = -269)$ for lumbar.

If the residual is identified as a missing vertebrae, we add an additional location at the center of gravity of the residual and loop once more through the pipeline.

Vertebrae gap regressor

To check if the distances between a set of vertebrae locations (namely vertebrae gap) are consistent, we learn two forms of the vertebrae gap statistics. One is Gaussian distribution for each anatomic group, the other is linear regressors predicting the gap given either the previous, next or both side neighboring gaps of each group.

For the learned coefficients of the Gaussian distributed vertebrae gap, we have $(\mu = 16.77, \sigma = 2.18)$ for cervical, $(\mu = 23.32, \sigma = 3.55)$ for thoracic, and $(\mu = 32.68, \sigma = 2.84)$ for lumbar. A vertebra gap G_i is considered as a gap of two consecutive vertebrae when $\mu - 3\sigma < G_i < \mu + 3\sigma$.

We train three types of the regressors to predict the vertebrae gap : using the both-side neighboring gaps $G_i = m_1 * G_{i-1} + n_1 * G_{i+1} + K_1$, using the previous gap $G_i = m_2 * G_{i-1} + K_2$ or using the next gap $G_i = n_2 * G_{i+1} + k_3$. The latter two are intended for the top and bottom vertebrae gaps who do not have gaps from both sides. The learned coefficient can be found in Table.A1.

	m_1	n_1	k_1	m_2	k_2	n_2	k_3
Cer.	0.55	0.45	-0.08	0.92	2.40	0.98	-0.13
Thor.	0.57	0.44	-0.24	0.93	2.29	0.97	-0.07
Lum.	0.56	0.46	-0.73	0.95	1.96	0.96	0.23

TABLE A1: Learned coefficients of the vertebrae gap regressors.

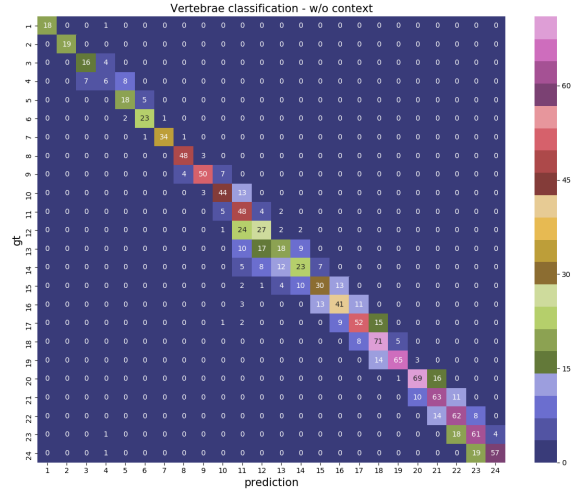
We then compute the Mean Relative Error (MRE) between the gap from the locations and the predicted gap from the regressor. The gap is considered as normal when $\mu_{mre} - 3 * \sigma_{mre} < MRE < \mu_{mre} + 3 * \sigma_{mre}$. The learned μ_{mre} and σ_{mre} for each anatomic group can be found in Table. A2.

	both sides		previous		next	
	μ_{mre}	σ_{mre}	μ_{mre}	σ_{mre}	μ_{mre}	σ_{mre}
cervical	9.13	2.86	10.20	2.05	12.13	3.36
thoracic	2.42	1.43	3.96	1.56	4.17	0.88
lumbar	2.04	0.93	4.45	1.55	5.16	1.71

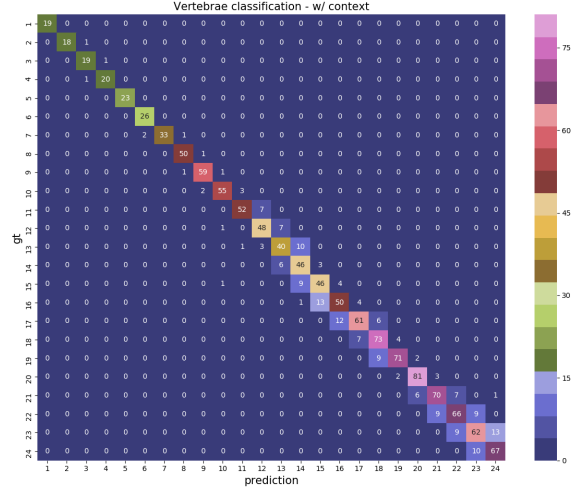
TABLE A2: MRE mean and standard deviation of the vertebra gap regressors.

If a gap is larger than the predicted range, we add an additional location in the middle of this gap and we loop again through the pipeline.

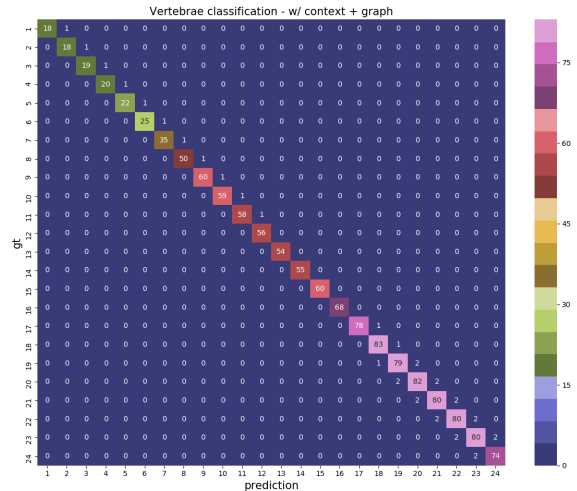
Appendix B. Vertebrae classification



(a) w/o context



(b) w/ context



(c) w/ context+graph

FIGURE B1: Confusion matrices of Individual vertebrae classification.